

Subscriber access provided by Brown University Library

Functional Nanostructured Materials (including low-D carbon)

Yb- and Mn-Doped Lead-Free Double-Perovskite Cs2AgBiX6 (X = Cl-, Br-) Nanocrystals

Na Chen, Tong Cai, Wenhao Li, Katie Hills-Kimball, Hanjun Yang, Meidan Que, Yasutaka Nagaoka, Zhenyang Liu, Dong Yang, Angang Dong, Cheng-Yan Xu, Rashid Zia, and Ou Chen ACS Appl. Mater. Interfaces, Just Accepted Manuscript • DOI: 10.1021/acsami.9b02367 • Publication Date (Web): 15 Apr 2019

Downloaded from http://pubs.acs.org on April 22, 2019

Just Accepted

"Just Accepted" manuscripts have been peer-reviewed and accepted for publication. They are posted online prior to technical editing, formatting for publication and author proofing. The American Chemical Society provides "Just Accepted" as a service to the research community to expedite the dissemination of scientific material as soon as possible after acceptance. "Just Accepted" manuscripts appear in full in PDF format accompanied by an HTML abstract. "Just Accepted" manuscripts have been fully peer reviewed, but should not be considered the official version of record. They are citable by the Digital Object Identifier (DOI®). "Just Accepted" is an optional service offered to authors. Therefore, the "Just Accepted" Web site may not include all articles that will be published in the journal. After a manuscript is technically edited and formatted, it will be removed from the "Just Accepted" Web site and published as an ASAP article. Note that technical editing may introduce minor changes to the manuscript text and/or graphics which could affect content, and all legal disclaimers and ethical guidelines that apply to the journal pertain. ACS cannot be held responsible for errors or consequences arising from the use of information contained in these "Just Accepted" manuscripts.



Yb- and Mn-Doped Lead-Free Double-Perovskite Cs_2AgBiX_6 (X = Cl⁻, Br⁻) Nanocrystals

Na Chen,^{†,‡} Tong Cai,[†] Wenhao Li,[§] Katie Hills-Kimball,[†] Hanjun Yang,[†] Meidan Que,[†] Yasutaka Nagaoka,[†] Zhenyang Liu,[†] Dong Yang,[#] Angang Dong,[¶] Chengyan Xu,[‡] Rashid Zia,[§] and Ou Chen^{*,†}

- [†] Department of Chemistry, Brown University, Providence, Rhode Island 02912, United States
- [‡] School of Materials Science and Engineering, Harbin Institute of Technology, Harbin, 150001, China
- § Department of Physics, Brown University, Providence, Rhode Island 02912, United States
- [#] Department of Macromolecular Science, Fudan University, Shanghai, 200433, China
- ¶ Department of Chemistry, Fudan University, Shanghai, 200433, China

Corresponding Author:

Email address: ouchen@brown.edu

ABSTRACT:

Lead-free double perovskite nanocrystals (NCs) have emerged as a new category of materials that hold the potential for overcoming the instability and toxicity issues of lead-based counterparts. Doping chemistry represents a unique avenue towards tuning and optimizing the intrinsic optical and electronic properties of semiconductor materials. In this study, we report the first example of doping Yb³⁺ ions into lead-free double perovskite Cs₂AgBiX₆ (X = Cl⁻, Br⁻) NCs via a hot injection method. The doping of Yb3+ endows the double perovskite NCs with a newly emerged nearinfrared emission band (sensitized from the NC hosts) in addition to their intrinsic trap-related visible photoluminescence (PL). By controlling the Yb3+ doping concentration, the dual emission profiles and photon-relaxation dynamics of the double perovskite NCs can be systematically tuned. Furthermore, we have successfully inserted divalent Mn²⁺ ions in Cs₂AgBiCl₆ NCs and observed emergence of dopant emission. Our work illustrates an effective and facile route towards modifying and optimizing optical properties of double perovskite Cs₂AgBiX₆ (X = Cl⁻ , Br) NCs with an indirect bandgap nature, which can broaden a range of their potential applications in optoelectronic devices.

KEYWORDS:

Lead-free double perovskite, Yb-doping, Mn-doping, indirect bandgap, dual emission, optical property

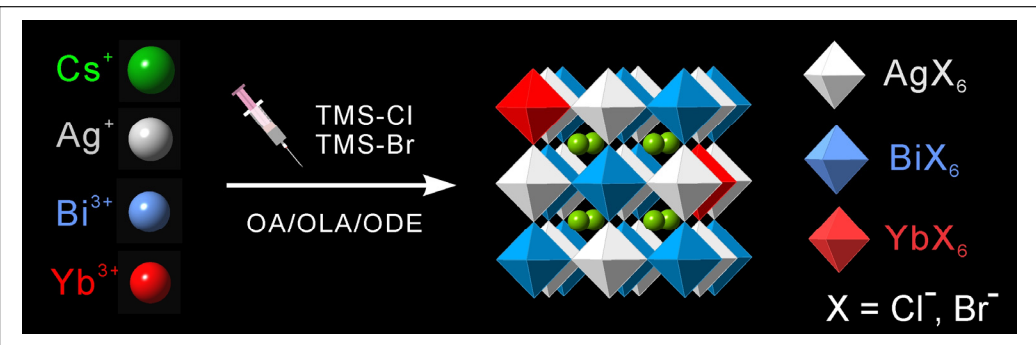
Introduction:

Lead halide perovskites have attracted extensive research interest due to their outstanding optoelectronic properties which render them as intriguing and promising semiconductor materials for a broad range of applications including photovoltaic devices, X-ray detection and conversion, solid-state lighting and displays. 1-11 Nevertheless, these intrinsic superior properties have yet to be fully realized in practical applications mainly due to the obstacles from the proverbial toxicity of Pb inclusion and poor materials stability. 12-15 Recent studies have suggested that substitution of two divalent Pb²⁺ ions with a pair of monovalent and trivalent metal ions in conventional lead-halide perovskites to form so-called double perovskite materials is an available option to alleviate both the toxicity and stability issues while maintaining three-dimensional (3D) perovskite structure and charge neutrality. 16-19 A significant amount of recent effort has been devoted to exploration of new synthetic methodologies and understanding of optoelectronic properties of various double perovskite materials. $^{20-24}$ In particular, the double perovskite Cs₂AgBiX₆ (X = Cl⁻, Br⁻) NCs have gained an increased amount of attention attributable to their long photogenerated carrier recombination lifetime, low carrier effective mass, and improved photo-, moisture- and thermal-stabilities.²⁵⁻²⁸ These combined merits signify them as promising alternatives to conventional lead-halide perovskites for future optoelectronic applications.²⁹⁻³²

Beyond conventional synthesis, doping 'impurities' in perovskite NCs is a unique

strategy towards expanding the compositional space of perovskite materials, oftentimes altering their optical and electronic properties in the ways inaccessible to their undoped counterparts.^{33,34} In this regard, rare earth and transition metal elements represent two important categories of elements that can be successfully doped into perovskite structures.³⁵⁻³⁸ Among them, Mn²⁺ and Yb³⁺ ions as dopant materials can induce additional dopant-related emission bands, resulting in a dual emission property. ³⁹⁻⁴¹ Especially, it has been shown that the ${}^2F_{5/2} \rightarrow {}^2F_{7/2}$ f-f transition of Yb³⁺ in an octahedral symmetry environment can offer a near infrared (NIR) emission (~1000 nm) with quantum cutting effect, permitted by the suitable energy offset between the incident and emitted photons.⁴² The quantum cutting process may allow the Yb-related NIR photoluminescence quantum yields (PL-QYs) to exceed unity, making them extremely attractive for a spectrum of applications, e.g., biological imaging and solar energy harvesting and conversion.⁴³ Despite these superior properties, doping in lead-free double perovskite systems remains largely unexplored. To the best of our knowledge, only two successful examples have been reported showing the incorporation of Yb³⁺ and Mn²⁺ ions in direct bandgap double perovskite Cs₂AgInCl₆ NCs. ^{44,45} Doping Yb³⁺ and Mn²⁺ ions in indirect bandgap double perovskite NCs has not yet been demonstrated.

In this work, we report the first example of Yb^{3+} and Mn^{2+} doped lead-free double perovskite Cs_2AgBiX_6 ($X = Cl^-$, Br^-) NCs with high crystallinity and morphological uniformity. For the Yb^{3+} doping case, we demonstrate that the Yb^{3+} ion can be doped



Scheme 1: Schematic illustration of the synthesis of Yb-doped double perovskite Cs_2AgBiX_6 ($X = Cl^-, Br^-$) NCs.

in both Cs₂AgBiCl₆ and Cs₂AgBiBr₆ NCs (Scheme 1). The doping concentration can be systematically controlled by adjusting the Yb-precursor amount during the synthesis. Optically, we show that a new NIR emission band centered at 1000 nm emerged resulting in a dual emission feature. The NIR emission peak has proved to be originated from an energy transfer process from the Cs_2AgBiX_6 (X = Cl⁻, Br⁻) NCs to the Yb-dopants, resulting in emission through the Yb³⁺ ${}^2F_{5/2} \rightarrow {}^2F_{7/2}$ f-f transition. Different PL intensity evolution trends for Yb-doped double perovskite NCs with different halides (i.e., Cl and Br) suggest that the energy transfer mechanisms are likely different for Cl and Br cases. Furthermore, we show that divalent Mn²⁺ ion can only be inserted into double perovskite Cs₂AgBiCl₆ NCs but not in Cs₂AgBiBr₆ NCs. Our study presented here demonstrates the feasibility of doping Yb³⁺ and Mn²⁺ cations into lead-free double perovskite Cs₂AgBiX₆ (X = Cl⁻, Br⁻) NCs, providing a unique system to exploit tunable dual emission and study the host-dopant interaction. We anticipate that our results can provide insights in delineating application-driven design rules for future lead-free double perovskite materials with expandable compositional space and tunable optoelectronic properties beyond the direct bandgap

materials.

Results and Discussion:

Yb-doped lead-free double perovskite Cs2AgBiX6 (X = Cl-, Br-) NCs were prepared using a modified hot-injection method via introducing Yb(C₂H₃O₂)₃•4H₂O into the reaction mixture (see SI for details). 46 In a typical synthesis, all metal (Cs, Ag, Bi, Yb) carboxylate precursors were first dissolved in 1-octadecene (ODE) together with oleic acid (OA) and oleylamine (OLA) as co-ligands. After vacuuming at 120 °C for 30 mins, chlorotrimethylsilane (TMS-Cl) or bromotrimethylsilane (TMS-Br) was swiftly injected into the heated metal salt solution at 145 °C to initiate nucleation and growth of NCs. The Yb-doped double perovskite NCs were immediately formed in seconds, and then collected from the cooled-down growth solution by centrifugation. Yb-doped Cs₂AgBiX₆ (X=Cl⁻, Br⁻) NCs with various doping concentrations can be achieved by adjusting the feeding amount of the Yb-precursor (see SI for details). By inductively coupled plasma atomic emission spectroscopy (ICP-AES), the actual doping concentrations of Yb3+ ions ([Yb]/([Bi]+[Ag]+[Yb])) in lead-free double perovskite Cs₂AgBiCl₆ (Cs₂AgBiBr₆) NCs were determined to be from 0.6 % (0.5 %) to 5.5 % (5.0 %) (Tables S1-3).

The electronic configuration of the Yb³⁺ ion, i.e., [Xe]4f¹³ endows it with an intricate optical property by producing a set of electronic energy levels that are sensitive to the local chemical environment of the Yb³⁺ ion.⁴⁷ Figure 1 presents representative room-temperature absorption, PL, PL excitation (PLE) spectra, and

transmission electron microscopy (TEM) images of double perovskite Cs₂AgBiX₆ (X = Cl⁻, Br⁻) NCs with the Yb³⁺ doping concentrations of 3.1 % (X = Cl⁻) and 2.9 % (X = Br⁻). Both samples exhibit a sharp absorption feature with the first electronic transition peak at 366 nm (3.40 eV) and 427 nm (2.91 eV) for Yb-doped Cs₂AgBiCl₆

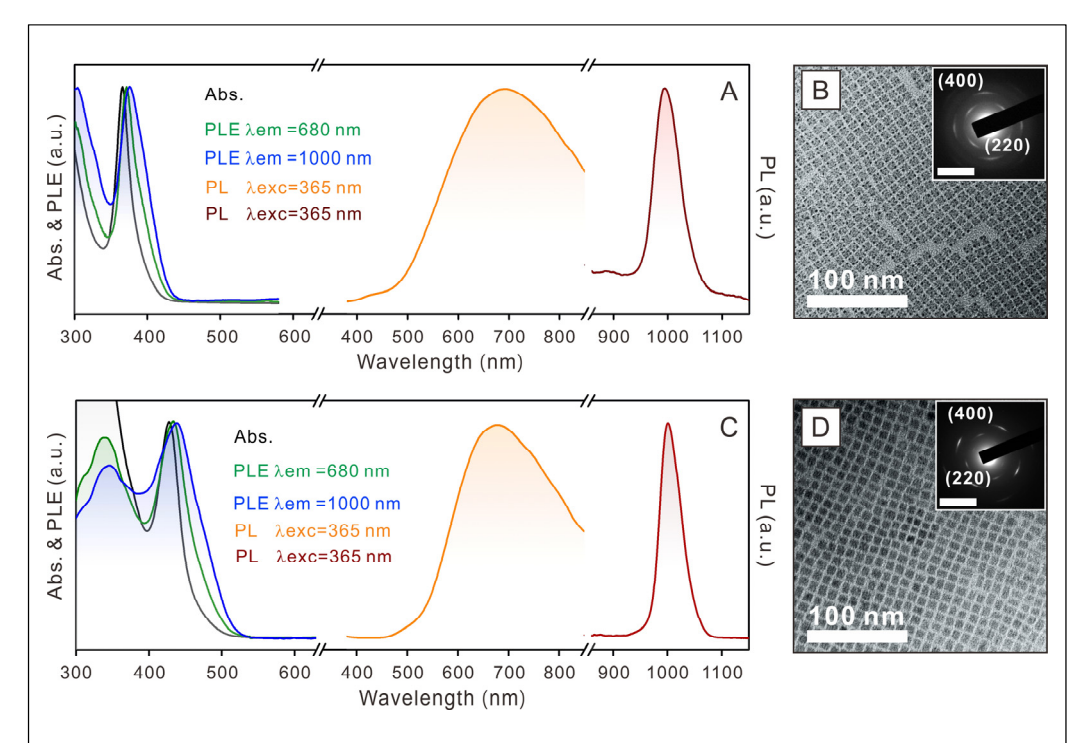


Figure 1: Optical and morphological data for Yb-doped double perovskite Cs_2AgBiX_6 (X=Cl⁻, Br⁻) NCs. The absorption (Abs.), PL and PLE spectra of Yb-doped $Cs_2AgBiCl_6$ NCs (Yb-doping concentration of 3.1%, A), and $Cs_2AgBiBr_6$ NCs (Yb-doping concentration of 2.9%, C). TEM images and SA-ED patterns (inset) of the corresponding Yb-doped $Cs_2AgBiCl_6$ NCs (B), and $Cs_2AgBiBr_6$ NCs (D). Inset: scale bar = 0.2 nm⁻¹.

and Cs₂AgBiBr₆ NCs, respectively (Figures 1A and C). The absorption spectra of doped NCs show similar peak positions and line-shapes to the undoped ones (Figures S1 and S2), consistent with the fact that the 6s-6p transition of the Bi³⁺ ions plays the dominating role in the first electronic transition of the double perovskite Cs₂AgBiX₆

NCs.²⁵ Our results indicate minimal electronic structure perturbations as a result of incorporation of guest Yb³⁺ ions (lack of 6p electrons) in the host double perovskite NCs, which also agreed well with previous observations for the Yb-doped CsPbCl₃ NCs.⁴⁸

Undoped double perovskite Cs₂AgBiX₆ (X = Cl⁻, Br⁻) NCs exhibit PL features with a broad weak emission peak (PL QY of ~ 0.3%, and full width at half maximum, FWHM of ~ 800 meV) centered around 680 nm (1.83 eV) (Figure S1 and S2). In addition, undoped samples show no any emission presence in 900-1200 nm wavelength range (Figure S3). The photo-recombination lifetimes determined by time-resolved PL spectroscopy are 33.4 ns and 5.7 ns for Cs₂AgBiCl₆ and Cs₂AgBiBr₆ NCs, respectively (Figure S4 and S5, Table S4 and S6). Unlike regular perovskite NCs, such as CsPbX3 systems, the PL peaks for Cs2AgBiCl6 and Cs₂AgBiBr₆ double perovskite NCs are more likely generated from the intra-band trap state related exciton recombination processes.^{25,49} The weak PL intensity is due to non-radiative pathways dominating the recombination mechanism of the photogenerated carriers (exciton).^{29,50} The ultrafast charge carrier trapping process can be responsible to the low PL QY in addition to the indirect bandgap of the materials. 19,25 Upon Yb³⁺ ion doping, while maintaining the visible trap-state emission, an additional narrow emission peak centered at 1000 nm (1.24 eV) emerged, resulting in a dual emission profile for both types of double perovskite NCs (i.e., Cs2AgBiCl6 and Cs₂AgBiBr₆ NCs). This newly emerged NIR emission is a characteristic ${}^2F_{5/2} \rightarrow {}^2F_{7/2}$

f-f transition of a Yb³⁺ ion in an octahedral coordination environment,³⁵ and unambiguously demonstrates the successful doping of Yb³⁺ ions by most likely replacing the native Bi³⁺ ions. A slight redshift (~ 12.5 -15.0 meV) of the Yb-emission peak as compared to that of the Yb-doped CsPbCl₃ NCs may be caused by photon energy loss by the lattice defects and strains originated from largely unbalanced sizes of neighboring octahedral units (AgX₆ vs YbX₆) in double perovskite lattices.^{42,43,48} The PLE spectra collected by monitoring the PL at 680 nm and 1000 nm closely follow the corresponding absorption profiles, implying that the Yb³⁺ emission is sensitized by the Cs₂AgBiX₆ (X = Cl⁺, Br⁻) NC host through an energy transfer process.^{44,51,52}

As revealed by TEM images (Figures 1B and D, and Figure S6), the Yb³⁺ doped double perovskite NCs show a cubic shape with an average edge length of \sim 8.0 \pm 0.6 nm for Yb-doped Cs₂AgBiCl₆ NCs, and \sim 7.9 \pm 0.7 nm for Yb-doped Cs₂AgBiBr₆ NCs. In both cases, the NC size decreased slightly as compared to their undoped counterparts (8.5 \pm 0.5 nm and 8.4 \pm 0.7 nm for Cs₂AgBiCl₆ and Cs₂AgBiBr₆ NCs, respectively, Figures S7 and S8). The slight reduction in size can be somewhat attributed to the lattice contraction of double perovskite NCs due to the replacement of Bi³⁺ ions (1.03 Å) by smaller Yb³⁺ ions (0.86 Å),⁵³ which is also reflected by the powder X-ray diffraction (XRD) results shown in Figure 2. Due to the high morphological uniformity of both samples, the lead-free double perovskite NCs can self-assemble into ordered monolayer lattices with localized selected-area electron

diffraction (SA-ED) signals (insets in Figure 1B and D). High resolution (HR) TEM images show that both the Yb-doped Cs₂AgBiCl₆ and Cs₂AgBiBr₆ NCs possess legible crystal lattices with interplanar distances of 0.27 nm and 0.28 nm, respectively (Figure S9). These lattice fringes match well to the (400) inter-plane distances of the corresponding double perovskite crystal phase, indicating the crystal structural

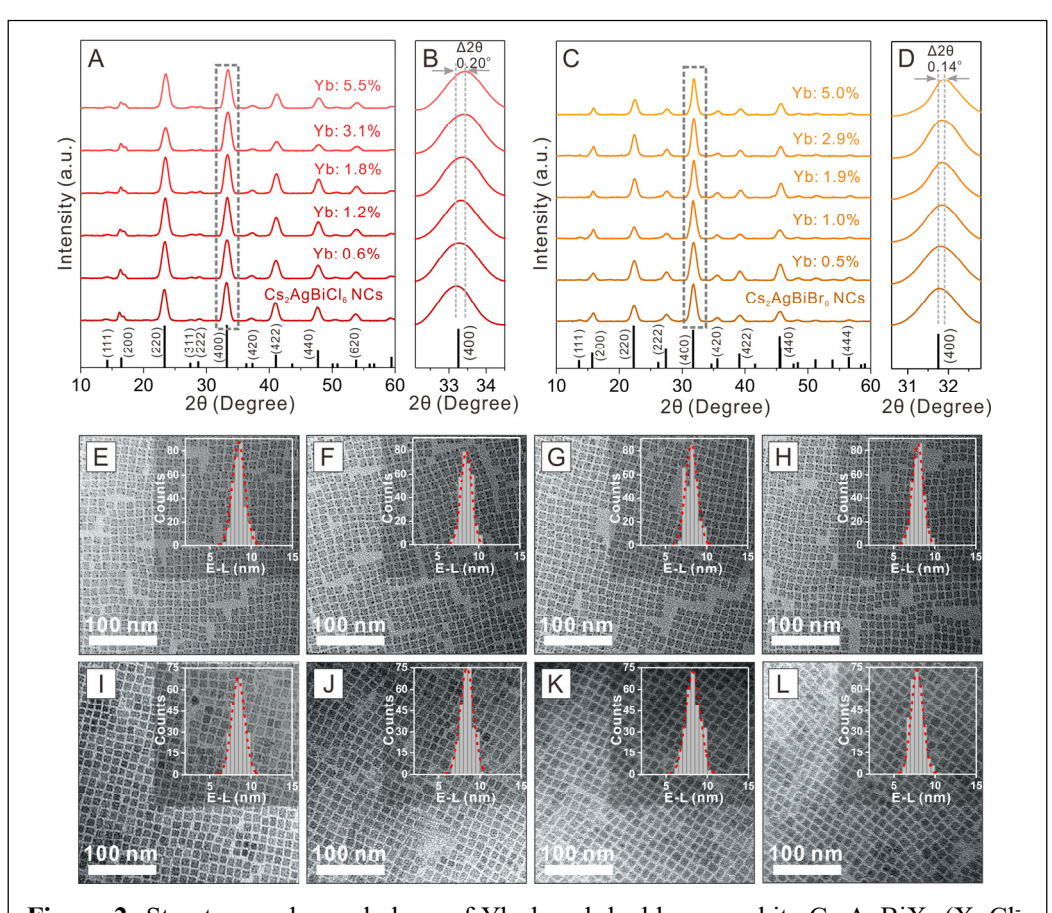


Figure 2: Structure and morphology of Yb-doped double perovskite Cs₂AgBiX₆ (X=Cl⁻, Br⁻) NCs. (A, C) Powder XRD patterns of Yb-doped Cs₂AgBiCl₆ NCs and Cs₂AgBiBr₆ NCs with different Yb³⁺ doping concentrations. (B, D) Zoomed-in XRD patterns for clear visualizations of the (400) diffraction peak. Standard diffraction patterns of Cs₂AgBiX₆ (X=Cl⁻, Br⁻) are provided for comparison (bottom black sticks). (E-H) TEM images of Yb-doped Cs₂AgBiCl₆ NCs with Yb³⁺ doping concentrations of 0.6 % (E), 1.2 % (F), 1.8 % (G), 5.5 % (H). (I-L) TEM images of Yb-doped Cs₂AgBiBr₆ NCs with Yb³⁺ doping concentrations of 0.5 % (I), 1.0 % (J), 1.9 % (K), 5.0 % (L).

integrity after Yb3+ ion doping.

The crystal phase of the double perovskite NCs were confirmed by XRD characterizations. The XRD patterns of Cs2AgBiX6 (X=Cl⁻, Br⁻) NCs without Ybdoping could be well indexed to a standard cubic double perovskite structure with a $Fm\overline{3m}$ space group and calculated lattice constants of 10.80 Å and 11.27 Å for Cs₂AgBiCl₆ and Cs₂AgBiBr₆ NCs, respectively (Figure 2A and C, Figures S10 and S16).⁵⁴ Upon doping Yb³⁺ ions, the XRD patterns showed identical crystal structure to that of the undoped NCs, as depicted in Figure 2A and C. Careful examination of the XRD patterns revealed that all the Bragg diffraction peaks monotonically shifted toward higher diffraction angles when increasing the Yb-dopant concentration (Figure 2, Figures S10-21 and Tables S8-19). For example, when monitoring the (400) peak, angle shifted 0.20° and 0.14° as compared to the undoped samples were observed when increasing the Yb concentration to 5.5% and 5.0% for Cs2AgBiCl6 and Cs₂AgBiBr₆ NCs, respectively (Figure 2B and D). These diffraction peak shifts, i.e., the lattice contractions, can be explained by the partial substitution of the larger Bi³⁺ ion (1.03 Å) with the smaller Yb3+ ion (0.86 Å).53 It is worth noting that, as compared to the undoped ones, the crystal structure of the double perovskite NCs does not show any appreciable changes after Yb³⁺ doping, even at the highest doping concentration studied in this work (Figure 2A-D). This high crystal phase stability can be explained by the same valence (3+) of the Yb-dopant ions and the Bi-host ions, as well as the acceptable ionic radius difference. Both factors allowed the Yb3+ ions to be immersed into the double perovskite Cs₂AgBiX₆ (X=Cl⁻, Br⁻) lattice while retaining their crystal structure. Identical cubic shape with minimal variations in size for the undoped and Yb-doped double perovskite NCs further confirmed the invariant nucleation and growth processes of the Yb-doped NCs.

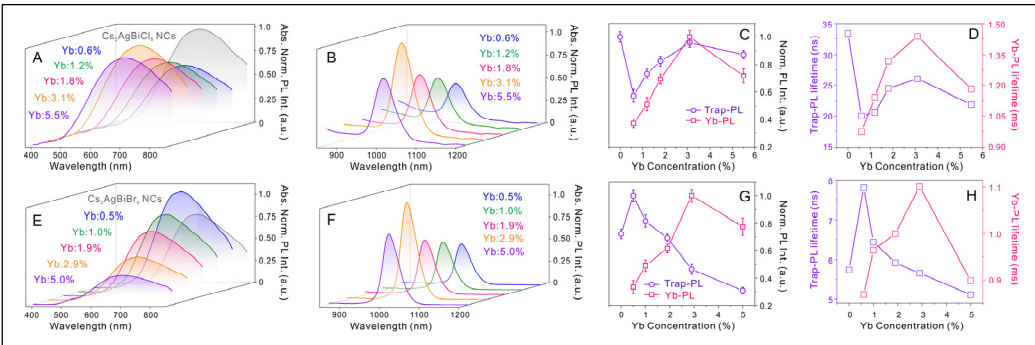


Figure 3: Normalized trap-state- and Yb-PL spectra of Yb-doped double perovskite Cs₂AgBiX₆ (X=Cl⁻, Br⁻) NCs with different doping concentrations. Yb-doped Cs₂AgBiCl₆ (A, B) and Cs₂AgBiBr₆ (E, F) NCs. Absorbance-normalized PL intensities as a function of Yb³⁺ doping concentration for Cs₂AgBiCl₆ (C) and Cs₂AgBiBr₆ (G) NCs. PL decay profile plotted as a function of Yb³⁺ concentration for Cs₂AgBiCl₆ (D) and Cs₂AgBiBr₆ (H) NCs.

Further, we have closely monitored the optical property variations of the Yb-doped double perovskite NCs at different doping levels. No obvious changes in absorption spectra were observed for the NCs with different Yb³⁺ doping concentrations (Figure S22 and S23), implying the electronic band structures of Cs₂AgBiX₆ (X=Cl⁻, Br⁻) NCs were not largely affected through doping.⁵⁵ However, different variation trends for the PL profiles were recorded for Yb-doped Cs₂AgBiCl₆ and Cs₂AgBiBr₆ NCs. In the Cs₂AgBiCl₆ case, the visible emission weakened distinctly (~ 33 % drop in intensity) after incorporating 0.6% Yb³⁺ ions (Figure 3A and C). Whereas, as increasing the Yb³⁺ doping concentration from 0.6% to 3.1%, both the trap-state- and Yb-PL

intensities gradually increased by 49% and 132%, respectively (Figure 3A-C). In parallel, time-resolved PL spectroscopy measurements on both emission bands showed the same lifetime prolongation trend (from 20.0 ns to 26.0 ns, and 0.97 ms to 1.44 ms for visible and NIR emission bands, respectively) (Figure 3D, Figure S4, Table S4-5). The simultaneous increase of both PL (trap-state- and Yb-PL) intensities indicates the suppression of non-radiative photo-relaxation channels in favor of radiative pathways. Detailed photon relaxation dynamics however need further investigation. The slow carrier dynamics of the NIR emission (at ms level) is consistent with the parity forbidden transition (${}^{2}F_{5/2} \rightarrow {}^{2}F_{7/2}$ f-f transition) of the Yb-PL, in line with previous observations for Yb-doped CsPbCl₃ NCs.^{48,56} Further increasing Yb³⁺ concentration to 5.5 %, however reduced intensity and shortened the lifetime for both visible and NIR emission bands (Figure 3A-D, Figure S4). This result is in accordance with the reported PL quenching effect induced by inter-dopant coupling at a high doping concentration.^{57,58}

In contrast to the matching trends for the intensity evolutions of both trap-state- and Yb-PL in Cs₂AgBiCl₆ NCs, opposite intensity progression trends were observed when doping Yb³⁺ in Cs₂AgBiBr₆ NCs. Specifically, upon doping 0.5% Yb³⁺ ions, a dramatic enhancement (~ 37% increase in intensity) of the visible PL as compared to that of the undoped sample was observed (Figure 3E and G). This is likely due to the suppression of non-radiative channels (e.g., surface and crystalline defects), thus hindrance of non-emissive energy loss, leading to an enhanced visible emission peak.

This dopant-induced PL intensity enhancement was also observed in other perovskite doping systems.^{33,44,59} The prolonged PL lifetime of the visible emission supports a partial removal of non-radiative photo-relaxation pathways (Figure 3H, Figure S5A, Table S6). When increasing the doping concentration from 0.5% to 5.0%, the visible emission intensity monotonically decreased to 31% of its highest intensity value (Figure 3E and G), and the corresponding photo-relaxation lifetime reduced from 7.8 ns to 5.1 ns (Figure 3H, Figure S5A, Table S6). Meanwhile, like the Cs₂AgBiCl₆ NC sample, the Yb-PL gradually increased until it reached its maximal intensity at the doping concentration of 2.9% and dropped to ~ 74% of the maximal intensity by further increasing the doping concentration to 5.0%. This Yb-PL intensity evolution trend was again coherent with Yb-PL lifetime changes (Figure 3H, Figure S5B, Table S7). These opposite intensity progression trends between the visible and NIR bands suggest a possible competing energy transfer mechanism from the conduction band of Cs₂AgBiBr₆ NC host to either the intra-band trap state or the Yb³⁺ ion center (²F_{5/2}) electronic state).⁴⁸

Beyond rare earth element doping, transition metals have proved to be capable of incorporating into perovskite structures, and consequently altering the optical, magnetic, and electronic properties of perovskites.⁶⁰⁻⁶⁴ Very recently, Manna et al. demonstrated the first example of Mn²⁺ ions doped into direct bandgap double perovskite Cs₂AgInCl₆ NCs, showing that the Mn-emission PL QY of as high as ~16%.⁴⁴ To demonstrate the feasibility of doping Mn²⁺ ions in indirect bandgap

double perovskite Cs₂AgBiX₆ NCs, we have synthesized Mn²⁺ ion doped Cs₂AgBiCl₆ NCs. Upon Mn²⁺ doping, the NC absorption profile remains nearly the same as the undoped sample with the first electronic transition peak centered at 366 nm (3.40 eV, Figure 4A). However, unlike the absorption, the PL spectral line-shape changed dramatically and can be fitted into two components (Figure 4B). The first component is a broad emission band (FWHM of ~ 820 meV) nearly identical to the emission profile of the undoped sample, which can be assigned to the NC intrinsic trap-state

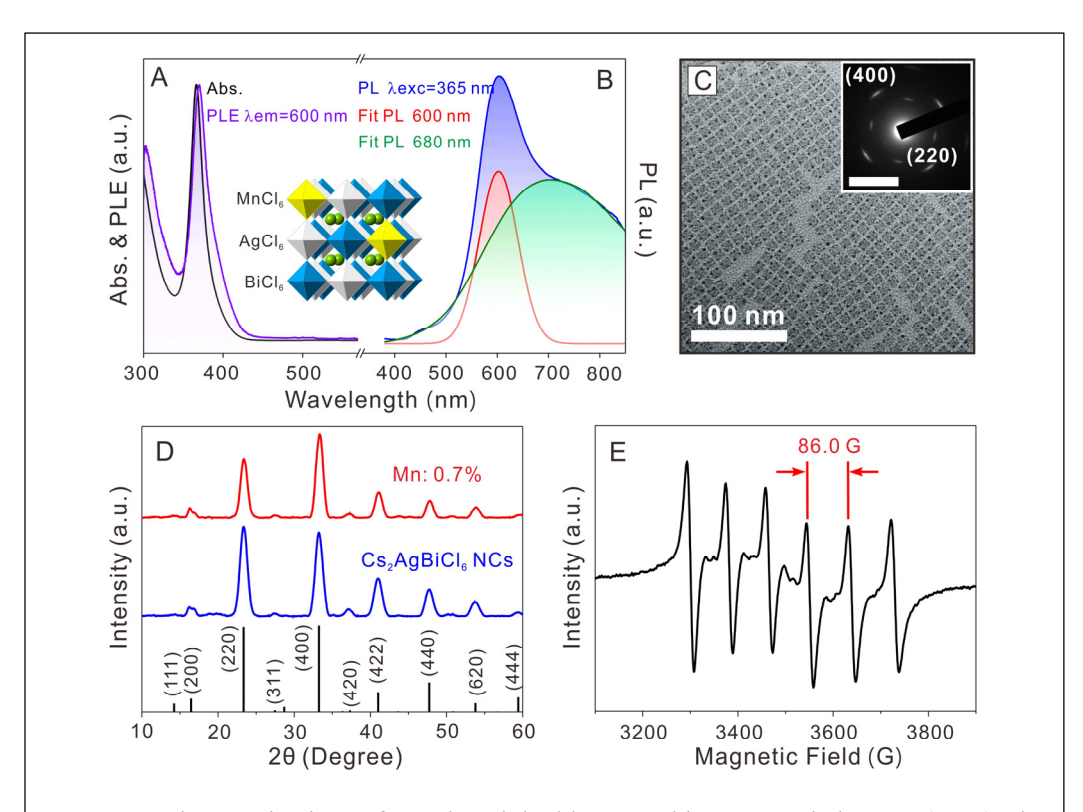


Figure 4: Characterizations of Mn-doped double perovskite Cs₂AgBiCl₆ NCs. (A, B) The absorption (Abs.), PLE and PL spectra of Mn-doped Cs₂AgBiCl₆ NCs. Inset: schematic of Mn-doped double perovskite Cs₂AgBiCl₆ NCs. (C) TEM image and SA-ED pattern (inset) of Mn-doped Cs₂AgBiCl₆ NCs with a Mn-doping concentration of 0.7%. Inset: scale bar = 0.2 nm⁻¹. (D) XRD patterns of Mn-doped (top) and undoped (bottom) Cs₂AgBiCl₆ NCs. Black sticks show the standard diffraction pattern of Cs₂AgBiCl₆ double perovskite. (E) EPR spectrum of the corresponding Mn-doped double perovskite Cs₂AgBiCl₆ NCs.

emission as we discussed above. However, the newly emerged secondary PL component with a relatively sharp peak profile centered at 600 nm (FWHM of ~ 300 meV) can be attributed to the ${}^4T_{1g} \rightarrow {}^6A_{1g} d^-d$ emission of Mn²⁺ ion centers. ${}^{65\text{-}67}$ A PL lifetime of 0.60 ms was obtained when measuring at 600 nm, agreed well with the assigned spin-forbidden transition of the Mn²⁺ ion centers. This result unambiguously proved that the Mn²⁺ ions have been successfully doped in the Cs₂AgBiCl₆ host NCs. The sample showed a low PL QY of less than 1%, consistent with the indirect bandgap nature of the host double perovskite Cs2AgBiCl6 NCs. 46 TEM measurement demonstrates that the Mn-doped Cs₂AgBiCl₆ NCs maintain good uniformity and a cubic particle shape with an average edge length of 8.5 ± 0.6 nm (Figure 4C and Figure S25A). The HR-TEM image displays a lattice fringe of 0.27 nm, corresponding to (400) plane of the double perovskite Cs₂AgBiCl₆ NCs (Figure S25B). No measurable shift in peak position can be observed from XRD patterns of Mn-doped and undoped Cs2AgBiCl6 NCs, which is likely due to the low doping concentration of Mn²⁺ ions in the Cs₂AgBiCl₆ NCs (0.7% determined by ICP-AES, Figure 4D, Figure S26 and Table S20). All these observations suggest that the crystallinity and morphology of Cs₂AgBiCl₆ NCs remained after doping with Mn²⁺ ions. Electron paramagnetic resonance (EPR) spectrum shows a well-defined six hyperfine splitting pattern due to the electron-nuclear spin coupling with a characteristic g-factor of 2.009 and a hyperfine coupling constant of 86.0 Gaussian (Figure 4E). 65,68 This EPR spectrum with a characteristic sextet and the observed coupling constant (i.e., 86.0 Gaussian) are signatures for represented Mn²⁺ ions positioned in an octahedral coordination environment,⁶⁹ unambiguously confirming the successful insertion of Mn²⁺ ions into the double perovskite lattice.⁴⁴ We attempted to dope Mn²⁺ ions into Cs₂AgBiBr₆ NCs under similar synthetic conditions to the Cs₂AgBiCl₆ case. However, neither optical data nor EPR measurements show evidence of successful Mn²⁺ ion incorporation.

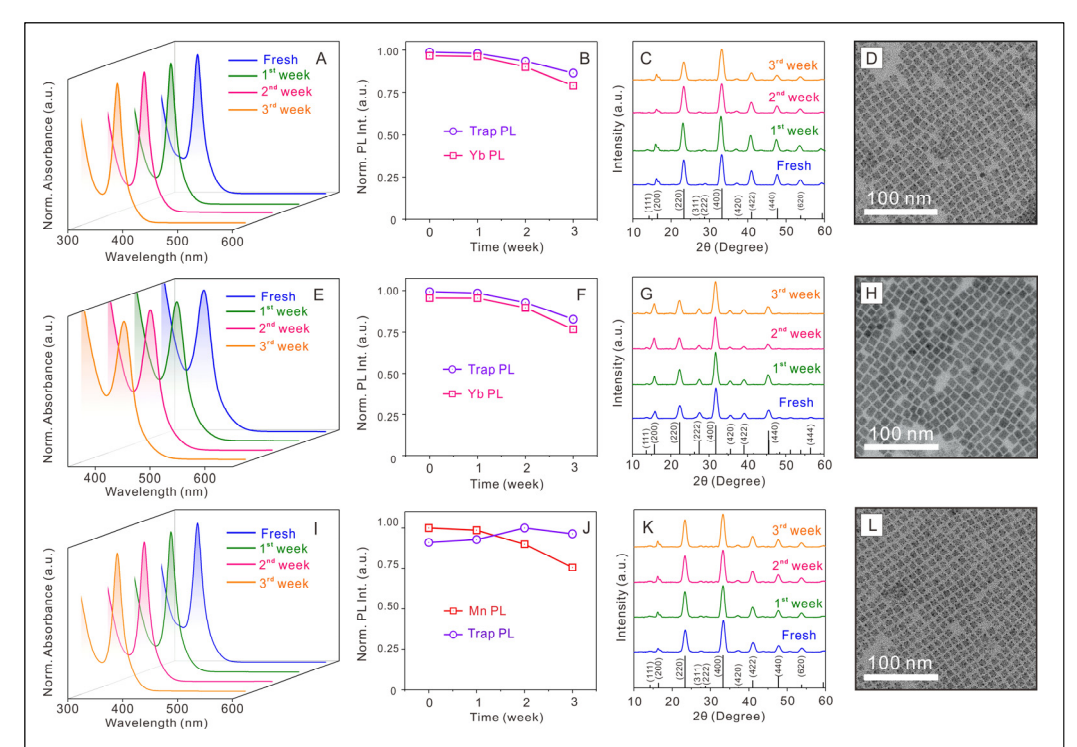


Figure 5: Optical, structural and morphological stabilities of the Yb- and Mn-doped double perovskite NCs. (A, E, I) Normalized absorption spectra (both the optical density and spectrum shape of the absorptions of NCs show nearly no change upon aging), (B, F, J) Normalized PL integrated intensity, (C, G, K) XRD patterns, and (D, H, L) TEM images of Yb-doped Cs₂AgBiCl₆ NCs (doping concentration of 3.1%), Yb-doped Cs₂AgBiBr₆ NCs (doping concentration of 2.9%) and Mn-doped Cs₂AgBiCl₆ NCs (doping concentration of 0.7%) at different storage time. TEM images show the NCs after 3-week storage under ambient conditions.

One of the advantages of double perovskites is their superior long-term stability as compared to the conventional lead-halide perovskites. 16 To evaluate the stability of the Yb- and Mn-doped double perovskite NCs, we monitored the optical, structural and morphological evolutions of the Yb-doped Cs₂AgBiX₆ (X=Cl⁻, Br⁻) NCs (doping concentrations of 3.1% and 2.9% for Cl⁻ and Br⁻ samples, respectively) and Mn-doped Cs₂AgBiCl₆ NCs (doping concentration of 0.7%) during long-term storage under ambient conditions. We found that all three samples showed nearly no change in their absorption spectra, XRD patterns, and particle size and shape for at least 3 weeks (Figure 5). In addition, PL spectra with dual emission features remained for all three samples, and with slight PL intensity decrease (~25%) during the same period of storage time (Figure 5B, F and J, Figure S27-29). These observations indicate that both the trivalent Yb and divalent Mn doping could support the double perovskite framework of Cs₂AgBiX₆ (X=Cl⁻, Br⁻) with respectable NC stability at least comparable to their undoped counterparts.^{20,70} The high stability of these NCs makes them suitable for various applications, e.g., photocatalysts, optoelectronics and photovoltaics as environmentally friendly halide double perovskites.

Conclusion:

In summary, we have successfully synthesized highly uniformed double perovskite Cs_2AgBiX_6 (X=Cl⁻, Br⁻) NCs doped with Yb³⁺ ions through a hot injection method. A dual emission profile (trap-state and Yb³⁺ ion emissions) can be observed upon doping. The NIR Yb-PL at 1000 nm is originated from an energy transfer from

Cs₂AgBiX₆ (X=Cl⁻, Br⁻) hosts to the ²F_{5/2} state of Yb³⁺ ion. We showed that the Yb³⁺ doping concentration can be controllably tuned by changing the precursor feeding amount during the synthesis. While maintaining the double perovskite crystal structure, the lattice constant shrunk monotonically upon increasing the Yb-dopant concentration. Interestingly, we observed distinct PL intensity evolution trends for the Cs₂AgBiCl₆ and Cs₂AgBiBr₆ NCs. We demonstrated that our synthetic method can be extended to the synthesis of Mn²⁺ doped Cs₂AgBiCl₆ NCs. Finally, we showed that these Yb- and Mn-doped double perovskite NCs exhibited superior long-term stability under ambient conditions. Our studies presented here verify the feasibility of doping lead-free double perovskite NCs even with an indirect bandgap structure. This doping technique may further expand the compositional space and alter the optoelectronic properties of lead-free double perovskites for their future applications.

ACKNOWLEDGMENTS

O. C., R. Z., and W. L. acknowledge support from the National Science Foundation (OIA-1538893). O. C. acknowledges the support from the Brown University startup fund and seed fund from the Brown Institute for Molecular and Nanoscale Innovation (IMNI). D. Y., and A. D. acknowledge support from the Senior Visiting Scholar Foundation of Key Laboratory at Fudan University K. H-K. is supported by the U.S. Department of Education GAANN research fellowship (P200A150037). TEM measurements were performed at the Electron Microscopy Facility in the Institute for

Molecular and Nanoscale Innovation (IMNI) at Brown University.

Supporting Information Available:

Details of NC synthesis and characterization, including the optical properties (absorption, PL and PLE spectra), TEM and HR-TEM images, and XRD analysis of undoped Cs₂AgBiX₆ (X=Cl⁻, Br⁻) NCs. The absorption, PL spectra, HR-TEM images, time-resolved PL decay curves, ICP-AES results and XRD fitting patterns of Yb-doped Cs₂AgBiX₆ (X = Cl⁻, Br⁻) NCs. The PL spectra, HR-TEM image and XRD pattern for Mn-doped Cs₂AgBiCl₆ NCs. This Supporting Information is available free of charge via the Internet at http://pubs.acs.org

REFERENCES

- (1) Xing, G.; Mathews, N.; Sun, S.; Lim, S. S.; Lam, Y. M.; Grätzel, M.; Mhaisalkar, S.; Sum, T. C. Long-Range Balanced Electron-and Hole-Transport Lengths in Organic-Inorganic CH₃NH₃PbI₃. *Science* **2013**, *342* (6156), 344-347.
- (2) Liu, L.; Huang, S.; Pan, L.; Shi, L. J.; Zou, B.; Deng, L.; Zhong, H. Colloidal Synthesis of CH₃NH₃PbBr₃ Nanoplatelets with Polarized Emission through Self-Organization. *Angew. Chem., Int. Ed.* **2017**, *56* (7), 1780-1783.
- (3) Swarnkar, A.; Marshall, A.; Sanehira, E.; Chernomordik, B.; Moore, D.;

Christians, J.; Chakrabarti, T.; Luther, J. Quantum Dot–Induced Phase Stabilization of α-CsPbI₃ Perovskite for High-Efficiency Photovoltaics. *Science* **2016**, *354* (6308), 92-95.

- (4) Lv, L.; Xu, Y.; Fang, H.; Luo, W.; Xu, F.; Liu, L.; Wang, B.; Zhang, X.; Yang, D.; Hu, W. Generalized Colloidal Synthesis of High-Quality, Two-Dimensional Cesium Lead Halide Perovskite Nanosheets and Their Applications in Photodetectors. *Nanoscale* **2016**, *8* (28), 13589-13596.
- (5) Sanehira, E. M.; Marshall, A. R.; Christians, J. A.; Harvey, S. P.; Ciesielski, P. N.; Wheeler, L. M.; Schulz, P.; Lin, L. Y.; Beard, M. C.; Luther, J. M. Enhanced Mobility CsPbI₃ Quantum Dot Arrays for Record-Efficiency, High-Voltage Photovoltaic Cells. *Sci. Adv.* **2017**, *3* (10), eaao4204.
- (6) Jiang, S.; Luan, Y.; Jang, J. I.; Baikie, T.; Huang, X.; Li, R.; Saouma, F. O.; Wang, Z.; White, T. J.; Fang, J. Phase Transitions of Formamidinium Lead Iodide Perovskite Under Pressure. *J. Am. Chem. Soc.* **2018**, *140* (42), 13952-13957.
- (7) Song, J.; Li, J.; Li, X.; Xu, L.; Dong, Y.; Zeng, H. Quantum Dot Light-Emitting Diodes Based on Inorganic Perovskite Cesium Lead Halides (CsPbX₃). *Adv. Mater.* **2015**, *27* (44), 7162-7167.
- (8) Yang, H.; Zhang, Y.; Hills-Kimball, K.; Zhou, Y.; Chen, O. Building Bridges between Halide Perovskite Nanocrystals and Thin-Film Solar Cells. *Sustainable Energy Fuels* **2018**, *2* (11), 2381-2397.
- (9) Li, Z.; Kong, L.; Huang, S.; Li, L. Highly Luminescent and Ultrastable CsPbBr₃

Perovskite Quantum Dots Incorporated into A Silica/Alumina Monolith. *Angew. Chem.* **2017**, *129* (28), 8246-8250.

- (10) Zhu, H.; Cai, T.; Que, M.; Song, J. P.; Rubenstein, B. M.; Wang, Z.; Chen, O. Pressure-Induced Phase Transformation and Band-Gap Engineering of Formamidinium Lead Iodide Perovskite Nanocrystals. *J. Phys. Chem. Lett.* **2018**, *9* (15), 4199-4205.
- (11) Xing, G.; Wu, B.; Wu, X.; Li, M.; Du, B.; Wei, Q.; Guo, J.; Yeow, E. K. L.; Sum, T. C.; Huang, W. Transcending the Slow Bimolecular Recombination in Lead-Halide Perovskites for Electroluminescence. *Nat. Commun.* **2017**, *8*, 14558.
- (12) Liang, L.; Gao, P. Lead-Free Hybrid Perovskite Absorbers for Viable Application: Can We Eat the Cake and Have it Too? *Adv. Sci.* **2018**, *5* (2), 1700331.
- (13) Huang, H.; Bodnarchuk, M. I.; Kershaw, S. V.; Kovalenko, M. V.; Rogach, A. L. Lead Halide Perovskite Nanocrystals in the Research Spotlight: Stability and Defect Tolerance. *ACS Energy Lett.* **2017**, *2* (9), 2071-2083.
- (14) Hills-Kimball, K.; Nagaoka, Y.; Cao, C.; Chaykovsky, E.; Chen, O. Synthesis of Formamidinium Lead Halide Perovskite Nanocrystals through Solid-Liquid-Solid Cation Exchange. *J. Mater. Chem. C* **2017**, *5* (23), 5680-5684.
- (15) Nagaoka, Y.; Hills-Kimball, K.; Tan, R.; Li, R.; Wang, Z.; Chen, O. Nanocube Superlattices of Cesium Lead Bromide Perovskites and Pressure-Induced Phase Transformations at Atomic and Mesoscale Levels. *Adv. Mater.* **2017**, *29* (18), 1606666.

- (16) Bekenstein, Y.; Dahl, J. C.; Huang, J.; Osowiecki, W. T.; Swabeck, J. K.; Chan, E. M.; Yang, P.; Alivisatos, A. P. The Making and Breaking of Lead-Free Double Perovskite Nanocrystals of Cesium Silver-Bismuth Halide Compositions. *Nano Lett.* **2018**, *18* (6), 3502-3508.
- (17) Li, Q.; Wang, Y.; Pan, W.; Yang, W.; Zou, B.; Tang, J.; Quan, Z. High-Pressure Band-Gap Engineering in Lead-Free Cs₂AgBiBr₆ Double Perovskite. *Angew. Chem.* **2017**, *129* (50), 16185-16189.
- (18) Kamat, P. V.; Bisquert, J.; Buriak, J. Lead-Free Perovskite Solar Cells. *ACS Energy Lett.* **2017**, *2* (4), 904-905.
- (19) Han, K.; Yang, B.; Hong, F.; Chen, J.; Tang, Y.; Yang, L.; Sang, Y.; Xia, X.; Guo, J.; He, H. Colloidal Synthesis and Charge-Carrier Dynamics of Cs₂AgSb_{1-y}Bi_yX₆ (X: Br, Cl; 0≤y≤1) Double Perovskite Nanocrystals. *Angew. Chem., Int. Ed.* **2019**, *58* (8), 2278-2283.
- (20) Volonakis, G.; Filip, M. R.; Haghighirad, A. A.; Sakai, N.; Wenger, B.; Snaith, H. J.; Giustino, F. Lead-Free Halide Double Perovskites via Heterovalent Substitution of Noble Metals. *J. Phys. Chem. Lett.* **2016**, *7* (7), 1254-1259.
- (21) Shi, Z.; Guo, J.; Chen, Y.; Li, Q.; Pan, Y.; Zhang, H.; Xia, Y.; Huang, W. Lead-Free Organic-Inorganic Hybrid Perovskites for Photovoltaic Applications: Recent Advances and Perspectives. *Adv. Mater.* **2017**, *29* (16), 1605005.
- (22) Zhou, J.; Xia, Z.; Molokeev, M. S.; Zhang, X.; Peng, D.; Liu, Q. Composition Design, Optical Gap and Stability Investigations of Lead-Free Halide Double

Perovskite Cs₂AgInCl₆. J. Mater. Chem. A **2017**, 5 (29), 15031-15037.

- (23) Volonakis, G.; Haghighirad, A. A.; Milot, R. L.; Sio, W. H.; Filip, M. R.; Wenger, B.; Johnston, M. B.; Herz, L. M.; Snaith, H. J.; Giustino, F. Cs₂InAgCl₆: A New Lead-Free Halide Double Perovskite with Direct Band Gap. *J. Phys. Chem. Lett.* **2017**, *8* (4), 772-778.
- (24) Xiao, Z.; Du, K.-Z.; Meng, W.; Wang, J.; Mitzi, D. B.; Yan, Y. Intrinsic Instability of Cs₂In(I)M(III)X₆ (M= Bi, Sb; X= Halogen) Double Perovskites: A Combined Density Functional Theory and Experimental Study. *J. Am. Chem. Soc.* **2017**, *139* (17), 6054-6057.
- (25) Yang, B.; Chen, J.; Yang, S.; Hong, F.; Sun, L.; Han, P.; Pullerits, T.; Deng, W.; Han, K. Lead-Free Silver-Bismuth Halide Double Perovskite Nanocrystals. *Angew. Chem.* **2018**, *130* (19), 5457-5461.
- (26) Hoye, R. L.; Eyre, L.; Wei, F.; Brivio, F.; Sadhanala, A.; Sun, S.; Li, W.; Zhang, K. H.; MacManus-Driscoll, J. L.; Bristowe, P. D. Fundamental Carrier Lifetime Exceeding 1μs in Cs₂AgBiBr₆ Double Perovskite. Adv. Mater. Interfaces 2018, 1800464.
- (27) Meng, W.; Wang, X.; Xiao, Z.; Wang, J.; Mitzi, D. B.; Yan, Y. Parity-Forbidden Transitions and Their Impact on the Optical Absorption Properties of Lead-Free Metal Halide Perovskites and Double Perovskites. *J. Phys. Chem. Lett.* **2017**, *8* (13), 2999-3007.
- (28) Wu, C.; Zhang, Q.; Liu, Y.; Luo, W.; Guo, X.; Huang, Z.; Ting, H.; Sun, W.;

- Zhong, X.; Wei, S. The Dawn of Lead-Free Perovskite Solar Cell: Highly Stable Double Perovskite Cs₂AgBiBr₆ Film. *Adv. Sci.* **2018**, *5* (3), 1700759.
- (29) Slavney, A. H.; Hu, T.; Lindenberg, A. M.; Karunadasa, H. I. A Bismuth-Halide Double Perovskite with Long Carrier Recombination Lifetime for Photovoltaic Applications. *J. Am. Chem. Soc.* **2016**, *138* (7), 2138-2141.
- (30) Gao, W.; Ran, C.; Xi, J.; Jiao, B.; Zhang, W.; Wu, M.; Hou, X.; Wu, Z. High-Quality Cs₂AgBiBr₆ Double Perovskite Film for Lead-Free Inverted Planar Heterojunction Solar Cells with 2.2% Efficiency. *ChemPhysChem* **2018**, *19* (14) 1696-1700.
- (31) Yang, B.; Mao, X.; Hong, F.; Meng, W.; Tang, Y.; Xia, X.; Yang, S.; Deng, W.; Han, K. Lead-Free Direct Bandgap Double Perovskite Nanocrystals with Bright Dual-Color Emission. *J. Am. Chem. Soc.* **2018**, *140* (49), 17001-17006.
- (32) Chakraborty, S.; Xie, W.; Mathews, N.; Sherburne, M.; Ahuja, R.; Asta, M.; Mhaisalkar, S. G. Rational Design: A High-Throughput Computational Screening and Experimental Validation Methodology for Lead-Free and Emergent Hybrid Perovskites. *ACS Energy Lett.* **2017**, *2* (4), 837-845.
- (33) Yong, Z.-J.; Guo, S.-Q.; Ma, J.-P.; Zhang, J.-Y.; Li, Z.-Y.; Chen, Y.-M.; Zhang, B.-B.; Zhou, Y.; Shu, J.; Gu, J.-L. Doping-Enhanced Short-Range Order of Perovskite Nanocrystals for Near-Unity Violet Luminescence Quantum Yield. *J. Am. Chem. Soc.* **2018**, *140* (31), 9942-9951.
- (34) Lozhkina, O. A.; Murashkina, A. A.; Shilovskikh, V. V.; Kapitonov, Y. V.;

Ryabchuk, V. K.; Emeline, A. V.; Miyasaka, T. Invalidity of Band-Gap Engineering Concept for Bi³⁺ Heterovalent Doping in CsPbBr₃ Halide Perovskite. *J. Phys. Chem. Lett.* **2018**, *9* (18), 5408-5411.

- (35) Pan, G.; Bai, X.; Yang, D.; Chen, X.; Jing, P.; Qu, S.; Zhang, L.; Zhou, D.; Zhu, J.; Xu, W. Doping Lanthanide into Perovskite Nanocrystals: Highly Improved and Expanded Optical Properties. *Nano Lett.* **2017**, *17* (12), 8005-8011.
- (36) Zhou, Y.; Chen, J.; Bakr, O. M.; Sun, H.-T. Metal-Doped Lead Halide Perovskites: Synthesis, Properties, and Optoelectronic Applications. *Chem. Mater.* **2018**, *30* (19), 6589-6613.
- (37) Zhang, X.; Zhang, Y.; Zhang, X.; Yin, W.; Wang, Y.; Wang, H.; Lu, M.; Li, Z.; Gu, Z.; William, W. Y. Yb³⁺ and Yb³⁺/Er³⁺ Doping for Near-infrared Emission and Improved Stability of CsPbCl₃ Nanocrystals. *J. Mater. Chem. C* **2018**, *6* (37), 10101-10105.
- (38) Cai, T.; Yang, H.; Hills-Kimball, K.; Song, J.-P.; Zhu, H.; Hofman, E.; Zheng, W.; Rubenstein, B.; Chen, O. Synthesis of All-Inorganic Cd-doped CsPbCl₃ Perovskite Nanocrystals with Dual-Wavelength Emission. *J. Phys. Chem. Lett.* **2018**, *9* (24), 7079-7084.
- (39) Liu, W.; Lin, Q.; Li, H.; Wu, K.; Robel, I.; Pietryga, J. M.; Klimov, V. I. Mn²⁺-Doped Lead Halide Perovskite Nanocrystals with Dual-Color Emission Controlled by Halide Content. *J. Am. Chem. Soc.* **2016**, *138* (45), 14954-14961.
- (40) Kroupa, D. M.; Roh, J. Y.; Milstein, T. J.; Creutz, S. E.; Gamelin, D. R.

Quantum-Cutting Ytterbium-Doped CsPb(Cl_{1-x}Br_x)₃ Perovskite Thin Films with Photoluminescence Quantum Yields over 190%. *ACS Energy Lett.* **2018**, *3* (10), 2390-2395.

- (41) Wei, Q.; Li, M.; Zhang, Z.; Guo, J.; Xing, G.; Sum, T. C.; Huang, W. Efficient Recycling of Trapped Energies for Dual-Emission in Mn-doped Perovskite Nanocrystals. *Nano Energy* **2018**, *51*, 704
- (42) Zhou, D.; Liu, D.; Pan, G.; Chen, X.; Li, D.; Xu, W.; Bai, X.; Song, H. Cerium and Ytterbium Codoped Halide Perovskite Quantum Dots: A Novel and Efficient Downconverter for Improving the Performance of Silicon Solar Cells. *Adv. Mater.* **2017**, *29* (42), 1704149.
- (43) Luo, X.; Ding, T.; Liu, X.; Liu, Y.; Wu, K. Quantum-Cutting Luminescent Solar Concentrators Using Ytterbium-Doped Perovskite Nanocrystals. *Nano Lett.* **2018**, DOI: 10.1021/acs.nanolett.8b03966
- (44) Locardi, F.; Cirignano, M.; Baranov, D.; Dang, Z.; Prato, M.; Drago, F.; Ferretti, M.; Pinchetti, V.; Fanciulli, M.; Brovelli, S. Colloidal Synthesis of Double Perovskite Cs₂AgInCl₆ and Mn-doped Cs₂AgInCl₆ Nanocrystals. *J. Am. Chem. Soc.* **2018**, *140* (40), 12989-12995.
- (45) Lee, W.; Hong, S.; Kim, S. Colloidal Synthesis of Lead-Free Silver-Indium Double-Perovskite Cs₂AgInCl₆ Nanocrystals and Their Doping with Lanthanide Ions. *J. Phys. Chem. C* **2019**, *123* (4), 2665-2672.
- (46) Creutz, S. E.; Crites, E. N.; De Siena, M. C.; Gamelin, D. R. Colloidal

Nanocrystals of Lead-Free Double-Perovskite (Elpasolite) Semiconductors: Synthesis and Anion Exchange to Access New Materials. *Nano Lett.* **2018**, *18* (2), 1118-1123.

- (47) Bünzli, J.-C. G. Lanthanide Luminescence for Biomedical Analyses and Imaging. *Chem. Rev.* **2010**, *110* (5), 2729-2755.
- (48) Milstein, T.; Kroupa, D.; Gamelin, D. R. Picosecond Quantum Cutting Generates Photoluminescence Quantum Yields over 100% in Ytterbium-Doped CsPbCl₃ Nanocrystals. *Nano Lett.* **2018**, *18* (6), 3792-3799.
- (49) Yang, B.; Chen, J.; Hong, F.; Mao, X.; Zheng, K.; Yang, S.; Li, Y.; Pullerits, T.; Deng, W.; Han, K. Lead-Free, Air-Stable All-Inorganic Cesium Bismuth Halide Perovskite Nanocrystals. *Angew. Chem., Int. Ed.* **2017**, *56* (41), 12471-12475.
- (50) Bartesaghi, D.; Slavney, A. H.; Gélvez-Rueda, M. C.; Connor, B. A.; Grozema,
 F. C.; Karunadasa, H. I.; Savenije, T. J. Charge Carrier Dynamics in Cs₂AgBiBr₆
 Double Perovskite. J. Phys. Chem. C 2018, 122 (9), 4809-4816.
- (51) Nandha, N.; Nag, A. Synthesis and Luminescence of Mn-doped Cs₂AgInCl₆ Double Perovskites. *Chem. Commun.* **2018**, *54* (41), 5205-5208.
- (52) Creutz, S. E.; Fainblat, R.; Kim, Y.; De Siena, M. C.; Gamelin, D. R. A Selective Cation Exchange Strategy for the Synthesis of Colloidal Yb³⁺-Doped Chalcogenide Nanocrystals with Strong Broadband Visible Absorption and Long-Lived Near-Infrared Emission. *J. Am. Chem. Soc.* **2017**, *139* (34), 11814-11824.
- (53) Du, K. z.; Meng, W.; Wang, X.; Yan, Y.; Mitzi, D. B. Bandgap Engineering of Lead-Free Double Perovskite Cs₂AgBiBr₆ through Trivalent Metal Alloying. *Angew*.

Chem., Int. Ed. 2017, 56 (28), 8158-8162.

- (54) McClure, E. T.; Ball, M. R.; Windl, W.; Woodward, P. M. Cs₂AgBiX₆ (X= Br, Cl): New Visible Light Absorbing, Lead-Free Halide Perovskite Semiconductors. *Chem. Mater.* **2016**, *28* (5), 1348-1354.
- (55) Parobek, D.; Roman, B. J.; Dong, Y.; Jin, H.; Lee, E.; Sheldon, M.; Son, D. H. Exciton-to-Dopant Energy Transfer in Mn-doped Cesium Lead Halide Perovskite Nanocrystals. *Nano Lett.* **2016**, *16* (12), 7376-7380.
- (56) Dodson, C. M.; Zia, R. Magnetic Dipole and Electric Quadrupole Transitions in the Trivalent Lanthanide Series: Calculated Emission Rates and Oscillator Strengths. *Phys. Rev. B* **2012**, *86* (12), 125102.
- (57) Chen, D.; Fang, G.; Chen, X., Silica-Coated Mn-Doped CsPb(Cl/Br)₃ Inorganic Perovskite Quantum Dots: Exciton-to-Mn Energy Transfer and Blue-Excitable Solid-State Lighting. *ACS Appl. Mater. Interfaces* **2017**, *9* (46), 40477-40487.
- (58) Xu, K.; Lin, C. C.; Xie, X.; Meijerink, A. Efficient and Stable Luminescence from Mn²⁺ in Core and Core-Isocrystalline Shell CsPbCl₃ Perovskite Nanocrystals. *Chem. Mater.* **2017**, *29* (10), 4265-4272.
- (59) Yao, J.-S.; Ge, J.; Han, B.-N.; Wang, K.-H.; Yao, H.-B.; Yu, H.-L.; Li, J.-H.; Zhu, B.-S.; Song, J.-Z.; Chen, C. Ce³⁺-Doping to Modulate Photoluminescence Kinetics for Efficient CsPbBr₃ Nanocrystals Based Light-Emitting Diodes. *J. Am. Chem. Soc.* **2018**, *140* (10), 3626-3634.
- (60) Guria, A. K.; Dutta, S. K.; Adhikari, S. D.; Pradhan, N. Doping Mn²⁺ in Lead

Halide Perovskite Nanocrystals: Successes and Challenges. *ACS Energy Lett.* **2017**, *2* (5), 1014-1021.

- (61) Van der Stam, W.; Geuchies, J. J.; Altantzis, T.; Van Den Bos, K. H.; Meeldijk, J. D.; Van Aert, S.; Bals, S.; Vanmaekelbergh, D.; de Mello Donega, C. Highly Emissive Divalent-Ion-Doped Colloidal CsPb_{1-x}M_xBr₃ Perovskite Nanocrystals through Cation Exchange. *J. Am. Chem. Soc.* **2017**, *139* (11), 4087-4097.
- (62) Das Adhikari, S.; Dutta, S. K.; Dutta, A.; Guria, A. K.; Pradhan, N. Chemically Tailoring the Dopant Emission in Manganese-Doped CsPbCl₃ Perovskite Nanocrystals. *Angew. Chem.* **2017**, *129* (30), 8872-8876.
- (63) Navas, J.; Sánchez-Coronilla, A.; Gallardo, J. J.; Hernández, N. C.; Piñero, J. C.; Alcántara, R.; Fernández-Lorenzo, C.; Desireé, M.; Aguilar, T.; Martín-Calleja, J. New Insights into Organic-Inorganic Hybrid Perovskite CH₃NH₃PbI₃ Nanoparticles. An Experimental and Theoretical Study of Doping in Pb²⁺ Sites with Sn²⁺, Sr²⁺, Cd²⁺ and Ca²⁺. *Nanoscale* **2015**, *7* (14), 6216-6229.
- (64) Abdelhady, A. L.; Saidaminov, M. I.; Murali, B.; Adinolfi, V.; Voznyy, O.; Katsiev, K.; Alarousu, E.; Comin, R.; Dursun, I.; Sinatra, L. Heterovalent Dopant Incorporation for Bandgap and Type Engineering of Perovskite Crystals. *J. Phys. Chem. Lett.* **2016**, *7* (2), 295-301.
- (65) Mir, W. J.; Jagadeeswararao, M.; Das, S.; Nag, A. Colloidal Mn-Doped Cesium Lead Halide Perovskite Nanoplatelets. *ACS Energy Lett.* **2017**, *2* (3), 537-543.
- (66) Nag, A.; Chakraborty, S.; Sarma, D. To Dope Mn2+ in A Semiconducting

Nanocrystal. Am. Chem. Soc. 2008, 130 (32), 10605-10611.

- (67) Nag, A.; Sapra, S.; Nagamani, C.; Sharma, A.; Pradhan, N.; Bhat, S.; Sarma, D. A Study of Mn²⁺ Doping in CdS Nanocrystals. *Chem. Mater.* **2007**, *19* (13), 3252-3259.
- (68) De, A.; Mondal, N.; Samanta, A. Luminescence Tuning and Exciton Dynamics of Mn-Doped CsPbCl₃ Nanocrystals. *Nanoscale* **2017**, *9* (43), 16722-16727.
- (69) Zou, S.; Liu, Y.; Li, J.; Liu, C.; Feng, R.; Jiang, F.; Li, Y.; Song, J.; Zeng, H.; Hong, M. Stabilizing Cesium Lead Halide Perovskite Lattice through Mn (II) Substitution for Air-Stable Light-Emitting Diodes. *J. Am. Chem. Soc.* **2017**, *139* (33), 11443-11450.
- (70) Huang, G.; Wang, C.; Xu, S.; Zong, S.; Lu, J.; Wang, Z.; Lu, C.; Cui, Y. Postsynthetic Doping of MnCl₂ Molecules into Preformed CsPbBr₃ Perovskite Nanocrystals via A Falide Exchange-Driven Cation Exchange. *Adv. Mater.* **2017**, *29* (29), 1700095.

TOC:

